Development of a Penta-Phase Brushless DC Hub-Motor

Petronio Vieira Jr.*, M. Godoy Simões
University of Sao Paulo
CEP: 05508-900 - Sao Paulo, SP – Brazil
mgs@usp.br

***Abstract* – Direct-drive high torque wheel motors have been showing advantages for electric vehicle (EV) applications as lower bearing and gearing losses, better transmission, fault tolerance, and less suspension struts requirements. This paper shows the development of a 3.2 HP five-phase dc-brushless wheel-motor to be embedded in the wheel hub of an EV. The machine has been designed analytically through project equations and curvilinear elements based analysis. An inspection has been made with a simulation study based on finite elements with the FLUX2D package. A dynamic model implemented in Simulink/MATLAB environment in order to help the design the control strategy has validated the torque loop control.**

I. INTRODUCTION

The electric vehicles research and development has been showing promises in several performance improvements for machines, drive systems and control [1] [2]. Custom-made electric machines are usually employed aiming optimization of efficiency, weight, volume and wide range control [3] [4]. Direct-drive motors with high torque wheel motor have been experimented in solar powered cars, indicating advantages as lower transmission, bearing and gearing losses, better fault tolerance figures and less mechanical transmission and suspension struts to the expenses of a trade-off unsprung weight effects. This paper shows the development of a penta-phase brushless dc machine to be embedded in the wheel hub of an electric vehicle.

II. ELECTROMECHANICAL DESIGN

Cylindrical shapes are common for such type of motor, depending how the magnetic field travels across the air-gap the construction is defined to be axial or radial. A radial flux machine has the advantages of higher field intensity across the stator windings due to a better magnetic path and utilization of standard rectangular magnets, easier to handle. Table I shows the nameplate design motor parameters and Fig. 1 the five phases machine diagram for a two poles section. Even though in an EV application like this, the nominal inertia is very high and the torque ripple is not critical, a high number of poles contributes for reducing the torque ripple and yields a smaller magnetic yoke, decreasing volume and weight, which is important. The magnet area physically limits the maximum number of poles. A five-phase machine allows better power utilization, decreasing total copper weight and the mutual inductance decoupling which contributes for a simplified analytical dynamic control modeling. A higher number of phases is only possible with more slots and a bigger diameter, so there is a trade-off decision dependent on the physical size of the motor. The exterior rotor was designed to have 216 NdFeB *Vacodyn 344 HR* magnets with high remanence (1.1T) and coercivity (1275 kA/m) on the inside surface and concentrated windings on the stator. The mechanical project took account of temperature rise to avoid demagnetization effects, exposition to road shocks, spills, dust and particles, and force demands on the wheel and tire. Special care has been taken on such aspects, but the mechanical design is out of the scope of this paper. Fig. 2 shows a photography depicting the stator and rotor construction.

Table I
Motor Parameters

Diameter: 275 mm
Length: 130 mm
Power rating: 3.2 HP
Poles: 12
Phases: 5
Nominal voltage: 133 V
Nominal current: 7.45 A
Rated speed: 750 RPM
Rated torque: 30 Nm

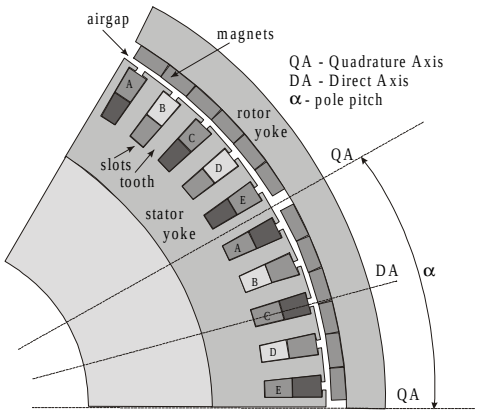

Fig. 1. Five phase brushless dc machine

The air-gap is not fully homogenous for the magnets are rectangular shaped and the flux distribution is uniform with leakage between poles as indicated on Fig. 3 showing a curvilinear elements based analysis which determined the flux correction factor KF = 0.92. Rectangular slots introduce harmonics and cogging torque, which can be

*Petronio Vieira Jr. is in leave of absence from University of Pará – Brazil

minimized by pole-shoe skewing. The skewing reduces the back emf and increases the ohmic losses, and can be compensated by proportionally decreasing the slot pitch. The amount of skew must be also optimized to minimize thrust load to the rotor bearings. Adhesive bonding the rotor magnets to the yoke surface has been calculated to have a parasitic influence of less then 1 %.

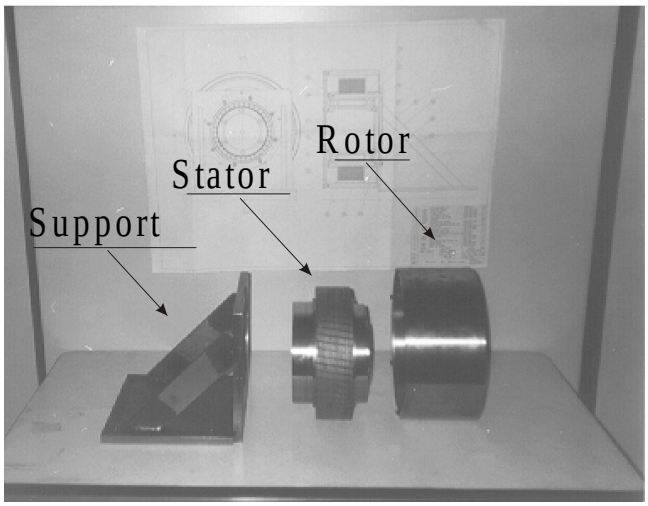

Fig. 2: Motor stator and rotor parts with support for workbench development

The prior analysis indicated the lateral and frontal leakages required for the net flux 10.5% higher than the effective flux. A path-vertex approach was applied along the magnetic path to compute the total magnetomotive force (MMF). The intersection of the permanent magnet flux with the motor net flux is depicted in Fig. 4 with the indication of the machine quiescent operating point.

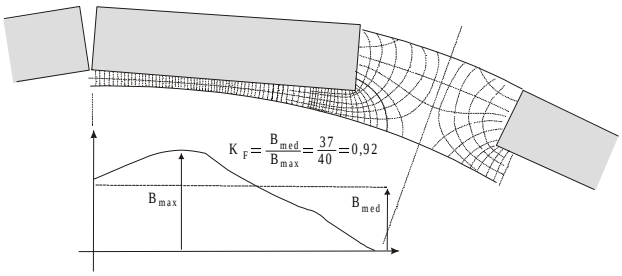

Fig. 3. Air-gap flux and effective correction factor

There are 60 slots with 12 coils for each phase. Each slot has two coils in a double-layer lap winding construction. Four phases are switched at same time carrying 7.45 A of nominal current, the wire gage has area of 3.11 mm^2, resistance of 0.041Ω, leading to 93.3% maximum efficiency.

The self inductance is related to the contribution of back iron, air-gap, slots and the end turns, given by Equ (1) – (3). Fig. 5 shows the dimension details for inductance computation. The self-inductance per phase is 1.08 mH with time constant of 6.5 msec.

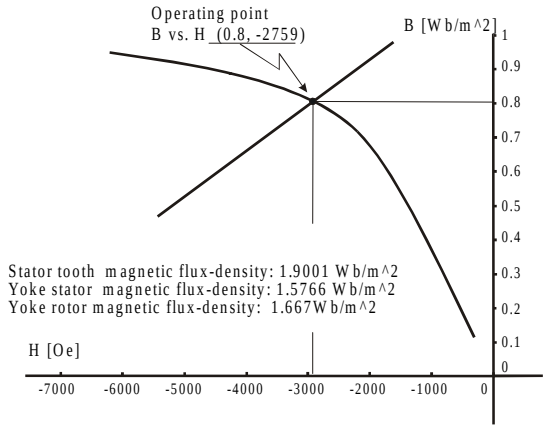

Fig. 4. Machine quiescent operating point

$$L_g = \frac{\pi \ \mu_o N_f^2 L \ r}{2 \ p^2 \left(g \ \frac{L_{mag}}{1.05} \right)} \quad \text{(Air-gap)} \quad (1)$$

$$\lambda_c = \frac{2 \ h_2}{(b_2 + b_3)} \frac{b_1}{h_2} \quad \text{(Slot)}$$

$$\lambda_b \cong \frac{L_{fr}}{L} \left[0.23 \ \log_{10} \left(\frac{L_{fr}}{S} \right) + 0.07 \right] \text{(End turn)}$$

$$\lambda_t \cong \log_{10} \left(1 + \frac{\pi}{2} \frac{L_t}{L_s} \right) \text{(Tooth)}$$

$$L_d = \mu_0 (\lambda_c + \lambda_t + \lambda_b) L \ Z_s^2 2 \ p \quad (2)$$

$$L_a = L_g + L_d = 1{,}08 \ 10^{-3} \frac{H}{\text{phase}} \quad (3)$$

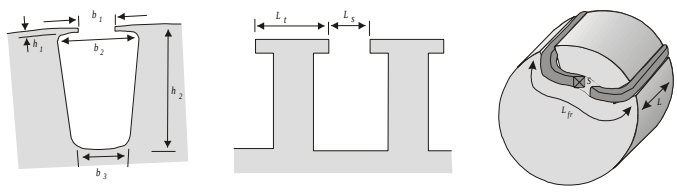

(a) (b) (c)

Fig. 5. Parameters for inductance calculation, (a) slot, (b) tooth, (c) end-turn

III. FEA AND DYNAMIC MODELING

A finite element analysis (FEA) of the motor was carried out with a 2D FE computer package following the procedure (A) – (C):

A. Pre-processing

Consisting of: (I) Conception of the geometric model of the motor according to the initial design configuration.

The model includes a rotor core with 72 magnets, air-gap and a stator core with 60 slots. Only a pair of poles has been modeled due to the symmetry. The size of the model was reduced to 10 slots and 12 magnets; (II) Mesh generation – a 2nd-order triangular elements is automatically generated (Fig. 6); (III) Assignment of physical properties - different materials were selected and assigned to the different regions defined in step (I); (IV) Specification of excitation sources - here, values of current sources are assigned to the coils (slots); (V) assignment of boundary conditions.

B. Solution step

After generating the FE mesh and assigning the physical properties to the model, a nonlinear system of equations is assembled and solved.

C. Post-processing

The results of simulations are visualized and analyzed through a set of graphics, curves (for instance, the flux density along the air-gap, and equipotential lines, color shades and vectors. Also, relevant global quantities can be computed, such as inductances, energy, forces, and so on.

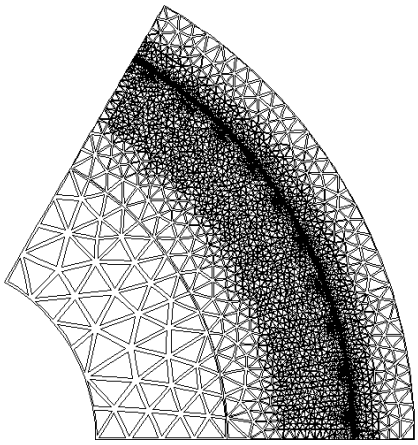

Fig. 6 Finite element mesh for one pair of poles

The back e.m.f. was obtained by simulating the no-load operating condition, i.e., no excitation source assigned to the winding.

Table II
Comparison of design parameters

	Analytical	*FEA*
Inductance	1,08 mH/phase	0,994 mH/phase
Pole linkage flux	2,92 10^{-3} Wb	2,67 10^{-3} Wb

The resulting magnetic field was only produced by the permanent magnets. In this case one can compute the flux per pole. To determine the inductance the simulation was performed so as to have only one phase of the stator winding fed and the magnets were replaced by air.

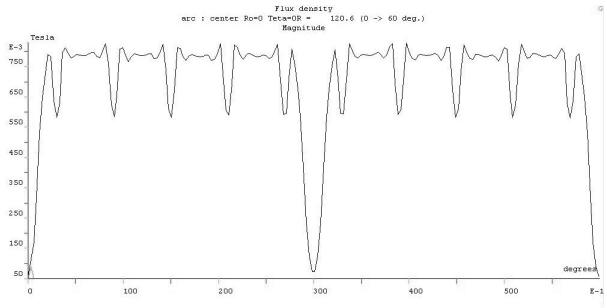

Fig. 7. Air-gap flux density showing maximum value: 0.826 T; average value: 0.704 T; RMS value: 0.726 T.

The FEA package needs the number of turns of the considered phase and yields to the value of the inductance. Table II shows the comparison between the analytical values and the ones found by FEA and Fig. 7 shows the air-gap flux density provided by FEA.

The dynamic modeling equations were derived to study the simulation operation in closed loop torque control with the machine/inverter topology given in Fig. 8; every 72° the power switching devices are commanded by a position sensor look-up table

Therefore, the forced and freewheeling current differential equations are switched and algebraically added to build up the machine terminal currents due to the imposed phase voltages.

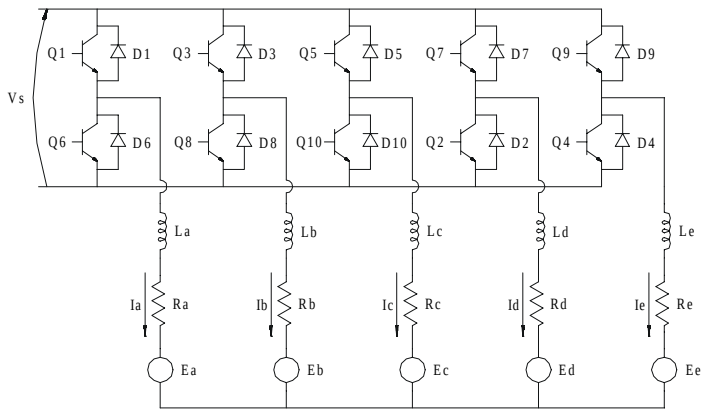

Fig. 8. Inverter and machine power circuit

Fig. 9 shows the complete dynamic model that was implemented in Simulink/MATLAB with the parameters, back-emf and torque computation formulated as the FEA analysis indicated. It is a scalar-based control approach where the PWM commands all the phases at the same time, depending on the PI correction of the instantaneous torque error.

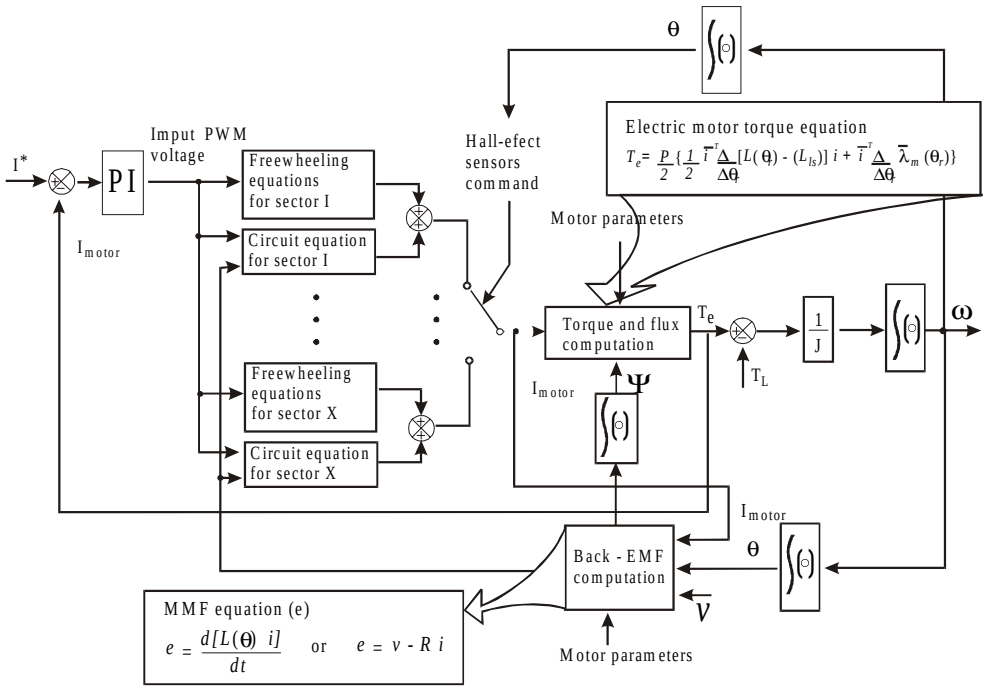

Fig. 9 Block diagram for dynamic simulation

The pulse-width-modulation can be implemented in two ways, by (a) modulating only the active device that is intended to be ON during the machine position sensor command where the decay of the current comes only from the free-wheeling diodes; or by (b) controlling the opposite devices at same time. The second approach forces a negative voltage (the machine has floating neutral), rapidly imposing phase currents as shown in Fig. 10.

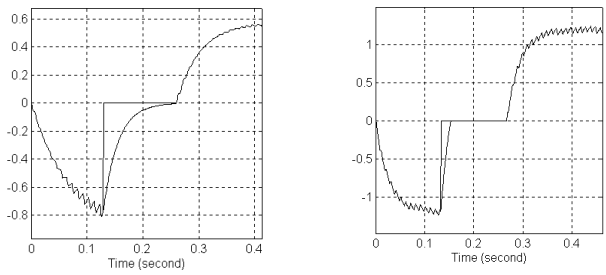

(a) (b)

Fig. 10: PWM strategies for phase current control, (a) using only freewheeling, (b) using full-bridge devices

The torque loop control of Fig. 9 was closed with an outer speed loop whose response is depicted in Fig. 11. It can be seen the machine speed and torque responses, and the phase currents.

IV. CONCLUSION

A 3.2 HP five-phase dc-brushless wheel-motor was designed analytically with project equations and curvilinear elements analysis and simulated by finite elements with the aid of FLUX2D package. There was a good match between the required parameters and FEA analysis, which helped to substantiate the dynamical motor model. The torque loop control was validated by a dynamic model implemented in Simulink/MATLAB environment in order to esigning the control strategy. The experimental implementation and performance studies are still in progress, and will be reported latter. A practical restriction that was not taken care on these previous studies was the temperature limitations for field applications. A second phase for this project is an optimized mechanical design, so as to fit a suitable refrigeration system.

V. ACKNOWLEDGEMENT

This project is being supported by FAPESP grant # 98/11351-7. The authors kindly acknowledge the suggestions given by J. C. Teixeira, I. Chabu and the help of R. F. Pereira. The FLUX2D package was possible due to the authorization of *CEDRAT Recherche* (Meylan-France) and the hands-on help given by Viviane C. Silva.

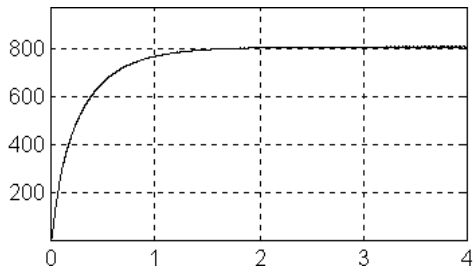

(a)

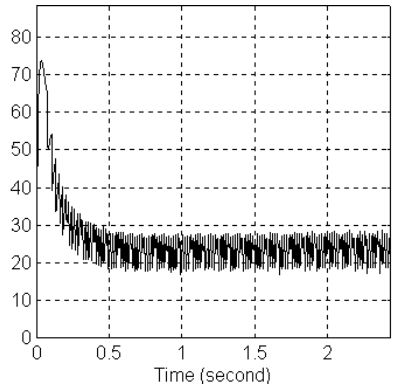

(b)

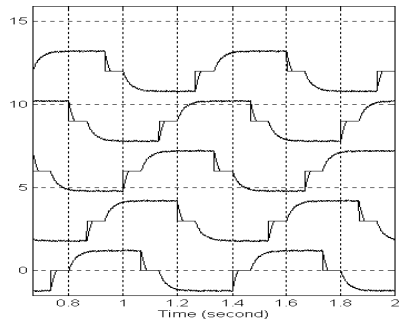

(c)

Fig. 11: Speed control, (a) Machine speed (RPM), (b) Torque response (Nm), (c) Phase currents (Amps) after steady-state

VI. REFERENCES

[1] G. H. Chen, K. J. Tseng, "Computer-aided design and analysis of direct-driven wheel motor drive," IEEE Trans. on Power Elect. vol. 12, pp. 517-527, May 1997

[2] D. Patterson, "Design and development of an axial flux permanent magnet brushless DC motor for wheel drive in a solar powered vehicle," IEEE Trans. on Ind. Appl. vol. 31, pp. 1054-1061, Sep/Oct 1995

[4] P. D. Evans, D. Brown, "Simulation of brushless DC drives," IEE Proceedings, Vol. 137, pp. 299 – 308, Sept. 1990

[5] P. Pillay, R. Krishnan, "Modeling of permanent magnet motor," IEEE Trans. on Ind. Elect. vol. 35, pp. 537 – 541, Nov. 1988

[6] A.K. Wallace, R. Spée, "The effects of motors parameters on the performance of brushless DC drives," IEEE Trans. on Power Electronics, vol. 5, pp. 2-8, Jan. 1990

[7] C.S. Berendsen, G. Champenois, A. Bolopion, "Commutation strategies for brushless DC motors: influence on instant torque," IEEE Trans. on Power Electronics, vol. 8, pp. 231 – 236, April 1993